PCCP
Physical Chemistry Chemical Physics

Accepted Manuscript

This article can be cited before page numbers have been issued, to do this please use: A. Banerjee and J. Shah, *Phys. Chem. Chem. Phys.*, 2025, DOI: 10.1039/D5CP02120K.

ROYAL SOCIETY OF CHEMISTRY

rsc.li/pccp

View Article Online
DOI: 10.1039/D5CP02120K

Elucidating Electronic and Structural Changes in Metal Porphyrins by 1-*n*-Alkyl-3-Methylimidazolium Cations

Atiya Banerjee and Jindal K. Shah*

School of Chemical Engineering, Oklahoma State University,

Stillwater, Oklahoma-74078

E-mail: jindal.shah@okstate.edu

Phone: +1 405-744-2295. Fax: +1 405-744-6338

View Article Online
DOI: 10.1039/D5CP02120K

Abstract

Metal porphyrins act as the reactive center of the ubiquitous monooxygenase, cytochrome P-450. As such, both their native and functionalized forms have been successfully utilized in studying biodegradation of a plethora of molecular substrates. Ionic liquids, although quite promising and possessing benign physicochemical properties, are poorly understood in terms of their biodegradability from a theoretical standpoint. In this article, a quantum mechanical treatment of ionic liquids 1-*n*-alkyl-3-methylimidazolium (n = 2, 4, 6, 8, and 10) ($[C_n\text{mim}]^+$) is carried out in the presence of a variety of metal porphyrins to understand their binding, which is the first step in the well-known catalytic cycle of cytochromes. Our treatment concerns the interaction strength between the cations and porphyrin molecules and we quantify it in terms of binding energy calculations of concerted electronic and geometrical effects. The conformations having the alkyl chain of these IL cations facing the porphyrin molecules are destabilized to the greatest extent as the chain length is enhanced along the homologous series. Structures of cation-porphyrin complexes are further analyzed by employing vibrational analysis on the active site molecules to deduce key structural features of the complexes. The reductive abilities of the metal porphyrins considered are also inferred by invoking conceptual DFT in our work through electrophilicity and Fukui reactivity indices. We uncover that the delocalized nature of the electrophilicity extends to the pyrrolic nitrogen atoms upon addition of an electron in the subsequent step to the binding. It is also surmised that geometrically, the core size is significantly affected upon inclusion of the cationic ligand with NiP showing the highest out of plane displacement. The motions governing the symmetry of the porphyrin macrocycle are perturbed from the native D_{4h} to D_{2h} in case of FeP, CoP, NiP and CuP exhibiting saddling and ruffling character and even B_{1u} and B_{2u} for MnP and ZnP showing doming character upon binding with $[C_n\text{mim}]^+$.

View Article Online
DOI: 10.1039/D5CP02120K

1 Introduction

Ionic liquids (ILs) are molten salts that consist of an asymmetric cation having an organic nature and a complementary anion that may be organic/inorganic. The combination of these ionic elements gives rise to structures and chemical entities, many of which exist in a liquid phase at ambient conditions. Due to their inherent characteristics such as extremely low vapor pressure and high design tunability, research on these chemicals has been very popular in the last two decades. They have been applied to a plethora of industrial applications employing their unique physicochemical properties.[1–15] Mixing one or more of these liquids have also been shown to emerge as a rational approach towards obtaining desirable properties.[16–22]

These ionic liquids have been projected to be environmentally friendly solvents due to their low volatility that contributes to lowering air pollution, if used at an industrial scale.[23–25] Despite the low potential for evaporation, their solubility in water[26] combined with limited biodegradability raises a concern that processes using ionic liquids could have a detrimental effect on aqueous and soil-related resources through significant carbon footprint.[27–29] Under the principles of green chemistry, the above fact demands a thorough assessment of their environmental effects[30–32] before they can be considered as benign chemicals.

Along this line, several investigations have been carried out to assess the structure-activity relationship of ionic liquids. Imidazolium-based ionic liquids bearing 1-*n*-alkyl-3-methylimidazolium cations[33,34] having side chain length six or higher ($n > 6$) have been shown to be partially degraded by microbial consortia[35–37] in an activated sludge environment. Several other works have also[38–41] highlighted the relationship between the alkyl chain length and the biodegradability of imidazolium-based ionic liquids. The reader is directed to excellent reviews composed over the last two decades for a comprehensive critique of the biodegradability of a variety of ionic liquids.[34,41–46]

Efforts have also been dedicated to understanding the mechanistic pathways by which ionic liquids undergo biodegradation based on analyses of intermediate metabolites. A number of authors

View Article Online
DOI: 10.1039/D5CP02120K

have suggested that the oxidation of cationic side chains mediates their degradation.[47–51] Multiple works have pointed out that the eventual degradation proceeds through suitable oxidation of the side chain for imidazolium[51] and pyridinium[38,52–54] ILs leading to simpler metabolites. This oxidation has been hypothesized to be linked to an appropriate alkyl monooxygenase such as cytochrome P-450 as enzymes such as the P-450 BM3 contains a metal-centered porphyrin macrocycle as its active site that is capable of oxidizing a wide range of substrates.[55–57]

The catalytic site in P-450 is the iron heme which contains iron at the center of a porphine ring,[58,59] which performs the oxidation reaction on the substrate within the binding pocket. All chemical reactions associated with the active site are implicitly related to the central metal ion.[60] Due to this reason, the modification of the porphyrin molecule has been of much interest in the creation of novel cytochromes[61] and artificial hemoproteins[62–64] to tune their reactivity. Out of these modifications,[65] the metals belonging to the row containing iron, such as Mn (Manganese), Copper (Cu), Nickel (Ni), Cobalt (Co) and Zinc (Zn) have been shown to be successfully synthesized[66] among many others. Our previous work[67] suggests that binding of 1-n-alkyl-3-methylimidazolium ($[C_n\text{mim}]^+$) cations to iron porphyrin (FeP) is conformationally dependent and the electronic properties reflect the conclusions drawn from the active model. The present work aims to understand the effect of substituting these metals into the active site of cytochrome P-450 on binding of $[C_n\text{mim}]^+$ cations as part of the crucial first binding step (Figure 1). The bound geometries have been analyzed in terms of the efficacy of the metal atom towards binding, geometrical changes induced by the cation on the active site and associated reactivity indices. To gain further insight into the complexation, a vibrational analysis consisting of some of the important modes of the metal porphyrins have also been exhibited.

View Article Online
DOI: 10.1039/D5CP02120K

2 Methodology

For this study, a range of metal substitutions were considered with the porphyrin macrocycle being kept intact. The six different metals studied in the work were namely, manganese (Mn), iron (Fe), cobalt (Co), copper (Cu), nickel (Ni), and zinc (Zn). All of the metal porphyrins were studied in bare form (metal porphyrins, MP) and in complexation with the imidazolium-based IL cations bearing 1-n-alkyl chain lengths (n = 2, 4, 6, 8, and 10) $[C_n mim]^+$.

To unravel binding modes of the ionic liquid cations as well as gauge the effect of the presence of different metals, geometry optimization was performed in the gas phase in complexation with metal porphyrins using the quantum mechanical Gaussian 09 software package.[68] All the atomic centers except the metal were treated with the well-known 6-31g(d,p) Pople basis set.[69] In our former publication,[70] we surmise the performance of adding a diffuse function (6-31+g(d,p)) to the existing 6-31g(d,p) basis set for non-metallic atoms in detail and conclude no significant changes compared to the original treatment. The LanL2DZ basis set,[71] shown to be highly efficient in handling transition metal-containing systems,[72–74] was employed to represent metal in MP and ionic liquid-MP complexes. Gas-phase ionic liquid cations, MP, and ionic liquid-MP complexes were subjected to geometry optimization using an advanced hybrid meta exchange-correlation functional M06,[75,76] capable of describing long-range dispersion corrections. Several publications[77–81] point towards the efficiency of the M06 functional in describing binding of small molecules, spin state energetics and absorption spectra over other variants M06-2X, M06L and M06HF.

Out of the possible multiplicities for these metal atoms, the one yielding the most stable porphyrin was considered for the analysis and in complexation with the ionic liquid cation.

2.1 Conformational Dependent Geometry Optimization

In order to assess the dependence of initial structures on the optimized geometries of ionic liquid-MP complexes, two different ionic liquid orientations relative to FeP were probed: tail-up (TU) and tail-down (TD) (Figure 2(a-b)). In our previous work,[67] we demonstrated that the TU and TD

View Article Online
DOI: 10.1039/D5CP02120K

conformations of ionic liquids are more informative for understanding the binding propensity of imidazolium-based ionic liquids with FeP. Furthermore, due to the vastly different nature of these two conformations, it is expected that they are likely to bracket additional local energy minima, if they exist. For $[C_n mim]^+$ cations, the TU conformations were generated by placing one of the hydrogen atoms attached to the carbon atom in the 3'-position at 3 Å from the metal atom underneath. On the other hand, TD conformations were constructed by positioning the cation in such a way that one of the H atoms attached to the terminal carbon in the side chain (1'- position) was 3 Å from the metal center. A similar strategy was followed to produce TD conformations for all the ionic liquid cations.

2.2 Binding Energy of Cation-Porphyrin Complexes

The binding energies between the imidazolium cation and the porphyrin molecules serve as an indicator of the stability of the overall complexation process. The binding energies of the ionic liquid-metal porphyrin complexes were calculated using eq. 1

$$\Delta E_{\text{binding}} = E_{\text{complex,cp}} - E_{\text{IL}} - E_{\text{MP}}. \quad (1)$$

In this equation, $\Delta E_{\text{binding}}$ refers to the binding energy of the complex; $E_{\text{complex,cp}}$ denotes the counterpoise corrected energy associated with the gas-phase optimized geometries of the complex and E_{IL}, E_{MP} are the gas phase energies of ionic liquid cation and the metal porphyrin, respectively.

In order to compare the stability of the two conformers for a given cation, the relative binding energies were calculated with respect to the minimum binding energy conformation (eq. 2)

$$\Delta\Delta E = \Delta E_{\text{binding}} - \Delta E_{\text{binding,min}} \quad (2)$$

where $\Delta E_{\text{binding,min}}$ is the energy of the most stable complex, i.e., the one exhibiting the highest absolute binding energy.

View Article Online
DOI: 10.1039/D5CP02120K

2.3 Electrophilicity Index

To understand the role of the imidazolium cation in changing the electronic environment of the porphyrin receptor, it is essential to understand the factors that are associated with the reactivity of the latter. In order to assess the propensity for the change in the oxidation state of the metal once the substrate, the imidazolium cation in this case, binds, electrophilicity was calculated as an indicator of porphyrin reactivity based on the frontier orbital energies. According to Parr et al.,[82] the electrophilicity ω can be obtained from the knowledge of the electron chemical potential μ and the chemical hardness η (Eq. 5).

$$\mu = \frac{E_{\mathrm{HOMO}} + E_{\mathrm{LUMO}}}{2} \tag{3}$$

$$\eta = E_{\mathrm{LUMO}} - E_{\mathrm{HOMO}} \tag{4}$$

$$\omega = \mu^2/2\eta \tag{5}$$

where E_{HOMO} and E_{LUMO} refer to the energies of the highest occupied molecular orbital (HOMO) and the lowest unoccupied molecular orbital (LUMO) for metal porphyrin in the complex. The HOMO and LUMO energies were calculated by performing a full population analysis on the converged geometry and then identifying the frontier energy levels for the porphyrin molecules in complex amongst the populated energy states using the software package GaussSum[83]

2.4 Fukui Indices

Fukui functions are significant in the understanding of local reactivity of a given atom in the scheme of the overall transfer of charge and electronic density in a chemical process. It presents a method from conceptual DFT to gauge the effect of an electron addition or removal process on a certain atom within the whole molecular framework. It is defined as the difference in the associated electronic density for the considered atom which can also be expressed locally as the difference in

View Article Online
DOI: 10.1039/D5CP02120K

the charges to condense the effects to a certain point. For an atom specific treatment of the reactive attack, the nucleophilic Fukui descriptor [84,85] was evaluated for the metal at the center of the active site molecule. This index is a measure of the propensity of a nucleophilic attack through a finite difference approximation involving atomic charges of the electron gaining metal center. The above described relationship is given as :

$$f^{+}_{M+Npy} = q_{M+Npy}(N+1) - q_{M+Npy}(N) \tag{6}$$

where the terms f^{+}_{M+Npy}, $q_{M+Npy}(N+1)$ and $q_{M+Npy}(N)$ represent the Fukui function for metal and the four pyrrole nitrogens in complex, the same charge computed after gaining an electron and the charge in the neutral state. This approach was formulated taking into consideration that electron transfer occurring on the metal ion undergoes significant redistribution to the four bound nitrogens in porphyrin. All the charges associated with the calculation were evaluated using the Hirshfeld scheme[86,87] on the geometry of the neutral species of the optimized cation-porphyrin complex to reflect the character of transfer of the electron density.

2.5 NBO Analysis

A donor-acceptor interaction analysis was performed by subjecting the optimized geometries to a natural population calculation using the natural bond orbital (NBO) method laid out by Weinhold and co-workers.[88–90] In this framework, second order perturbation analysis provides a description of the possible donor-acceptor orbital interactions within the entire molecule. The second order correction to the natural Lewis energy description is given by

$$\Delta E^{(2)}_{ij} = -q_i |F_{ij}|^2 / (\epsilon^{(NL)}_j - \epsilon^{(L)}_i) \tag{7}$$

where q_i is the occupancy of the donor orbital, F_{ij} is the sum of all effective one-electron hamiltonian operators and $(\epsilon^{(NL)}_j - \epsilon^{(L)}_i)$ represents the difference in the corresponding acceptor (NL) and donor orbital energy levels (L).

View Article Online
DOI: 10.1039/D5CP02120K

The stabilizing donor-acceptor energies resulting from the metal porphyrin to the cation were recorded in order to understand the strength of these interactions for different metals in order to provide insight into Lewis-type interactions. Furthermore, to probe the effect of the presence of either monomer on these energies, i.e. cation and metal, the net intermolecular stabilization was parsed into two components: (a) stabilization with metal orbitals as the donor orbitals and cation as the acceptor; (b) with cation acting as the donor and the metal as the receiver of electron density.

2.6 Vibrational Analysis and Core Size

Porphyrins have been identified to show distortions promoting non-planarity related to size change in the 4-N cavity in the overall macrocycle.[91] These changes have often been tied to their reactive properties such as electron transfer, axial ligation and redox potentials.[92,93] Among the possible deformations, ruffling and doming have been widely used as models to describe associated spectral properties.[94–96] The normal structure decomposition (NSD) analysis as described in Jentzen et al.[97,98] was utilized to account for the out-of-plane normal deformations in the porphyrin-cation complexes. Figure 3 describes these out-of-plane symmetric deformations, namely, saddling (B_{2u}), ruffling (B_{1u}), doming (A_{2u}), waving (($E_g(x)$) and ($E_g(y)$)) and finally, propellering (A_{1u}). The application of NSD analysis for quantitatively accounting for porphyrin distortion profiles have been reviewed in detail in Kingsbury and Senge.[99] The above described deformations were evaluated by extracting the coordinates of the energy minimized porphyrin macrocycle from the overall complex and recording the deformations belonging to each of the above mentioned symmetries for all of the associated structures. These distortion characteristics drive the structure of the porphyrin towards a specific symmetry and have the potential to act as a template for site specific design of chiral porphyrins. In the present work, the symmetric deformations in IL cation bound porphyrins have been quantified. The change in the porphyrin core size was determined by recording the change in the average metal-pyrrole nitrogen distance for the bare and cation-bound porphyrins.

View Article Online
DOI: 10.1039/D5CP02120K

3 Results and Discussion

The results section has been arranged in order to include, firstly the binding energy profile for all of the six metal porphyrins, followed by a discussion of electronic properties and analysis of key vibrational modes to provide physical insight into the complexation of IL cations with the six metal porphyrins.

3.1 Binding Energies

The possible spin states and relative energetics of the bare porphyrins are given in Table 1. As we move towards the $3d^5 - 3d^{10}$ configuration metals (Mn to Zn), MnP exhibits a high-spinstable spin state as a sextet with five unpaired electrons, while FeP occupies the intermediate triplet state as discussed in Banerjee and Shah.[67,70] On the other hand, the remaining four metal porphyrins reside in their lowest spin state: CoP and CuP are doublets while NiP and ZnP are singlet species. The relative energies from optimized geometries of these porphyrins at possible spin states show significant favorability for the ground state over the others (Tables S1- S5). Our observations for these spin states align with the work reported by Feng et al.[100] in which they considered 11 different divalent porphyrins with and without complexation with an axial pyridine ion.

Binding energies of each of the metal porphyrins to the imidazolium cation is given in Figure 4 and their combined profile is displayed in Figure S6, while relative energies are reported in Table 2. Our previous work suggested that binding, in case of FeP, is conformationally dependent as the alkyl chain length of the cation is enhanced and the major contribution to the total binding energy comes from interaction energies. The reader is referred to our previous work [67] for a detailed discussion on the binding energetics, profiles and reductive ability of FeP in the presence of $[C_n\text{mim}]^+$ cations ($n = 2, 4, 6, 8, 10$). All other metal porphyrins, except for FeP, will be discussed here.

View Article Online
DOI: 10.1039/D5CP02120K

For MnP bearing the $3d^5$ configuration, the range of binding energies are observed to be between -16.4 to -7.7 kcal/mol as the alkyl chain increases. Similar to our observations for $[C_n\text{mim}]$-$^+$FeP complexes, the binding strength reduces progressively for both the TU and TD conformations with TU complexes more preferred over TD conformations for $[C_n\text{mim}]^+$ with $n = 6, 8, 10$. The relative energies between the two conformations presented to the porphyrin are evaluated to be 1.4, 2.8 and 2.9 kcal/mol for the imidazolium cation bearing the hexyl, octyl, and decyl chain, respectively (Table 2).

The cation binding energy profiles obtained with $3d^7$ CoP are very similar to those calculated with MnP. Upon binding, there is an energy gain of anywhere between -16.9 kcal/mol to -8.0 kcal/mol with lower binding energies for longer alkyl chains. TU and TD complexes are nearly indistinguishable for $[C_2\text{mim}]^+$, $[C_4\text{mim}]^+$, and $[C_6\text{mim}]^+$ while the TD conformations are destabilized by 3.4 kcal/mol and 2.7 kcal/mol for $[C_8\text{mim}]^+$ and $[C_{10}\text{mim}]^+$.

For NiP, while the TU conformations yield binding energies between -17.4 and -11.6 kcal/mol, the TD binding energies range from -18.1 to -9.0 kcal/mol. Binding energies are within 1 kcal/mol for $[C_2\text{mim}]^+$ and $[C_4\text{mim}]^+$ cations for both TU and TD conformations, implying conformationally independent stability when the alkyl chain length is short. The conformational preference begins to dominate for longer alkyl chains with TU conformations are favored over the TD conformations for the rest of the homologous series. Differences in binding energies between TD and TU conformations for $[C_6\text{mim}]^+$, $[C_8\text{mim}]^+$, and $[C_{10}\text{mim}]^+$ are 1.7, 1,8, and 2.6 kcal/mol.

CuP binds to IL cations with energies in the range of -16.1 to -7.0 kcal/mol. The strength of binding of both TU and TD geometries individually reduce with the increase in the chain length of the cation. For $[C_2\text{mim}]^+$ and $[C_4\text{mim}]^+$ cations, binding energies are similar for both TU and TD conformations, while TU conformations are more stable for the remaining three cations.

View Article Online
DOI: 10.1039/D5CP02120K

Finally for ZnP complexes, the range of binding energies are -14.7 to -9.0 kcal/mol for TU complexes, and -13.4 to -6.7 in case of TD complexes. On a relative scale, the TD geometries are shown to be less favorable irrespective of the size of the chain length on the cation. The relative energies for chain lengths having 6, 8 and 10 carbon atoms are less favorable towards TD conformation by 3.6, 2.2 and 2.3 kcal/mol respectively.

Upon comparing the absolute binding energies for all the metal porphyrins, we conclude that NiP binds the strongest to a given IL cation for both sets of conformations. Geometrically, similar to our observation for FeP, TU conformations adopt a stacked conformation in which the plane of the imidazolium cation is parallel to that of the porphyrin enabling favorable $\pi - \pi$ interaction. TD geometries show a gradual displacement of the imidazolium ring away from the metal center of the porphyrin with the ring adopting a tilted conformation with respect to the porphyrin plane for $n \geqslant 6$. Selected geometries to illustrate this fact have been given in Figure 2(c-e) and complete set except Fe containing complexes are provided in the SI (Figures S1- S5). The presence of ionic liquid cations also induces distortions to a nearly perfect planar geometry of bare metal porphyrins. This will be discussed further in the section dedicated to core size and vibrational analysis. The magnitude of the binding energies obtained in this work is an order of magnitude lower than those calculated for anionic ligands,[101] implying a much less stable ligand-metal porphyrin complexation when the ligand is electron deficient.

3.2 Electrophilicity Index

Results from electrophilicity calculations are depicted in Fig. 5 for TU and TD conformations presented to all the ionic liquid-MP complexes. The electrophilicity index computed for all the porphyrins shows a trend similar to our previous work concerning the complexation of 1-n-alkyl-3-methylimidazolium cations with iron porphyrins in tail up and tail down geometrical modes. Specifically, the electron uptake ability of each of the metal porphyrins is enhanced in the presence of the positively charged cation. Figure 5 shows the individual electrophilicity index profiles for

View Article Online
DOI: 10.1039/D5CP02120K

each of the porphyrins considered in the work and it can be clearly seen the imidazolium cations almost make the uptake ability of the cation triple of its gas phase datum, enhancing the overall chemical potential of the complex. This is in line with our former works on FeP containing complexes bearing $[C_n mim]^+$ cations[67] and family of aromatic cations.[70] Across all of the porphyrins, the conformational effect of placing the alkyl chain is evident as the chain length on the imidazolium cation in increased to hexyl or greater. Upon considering the evaluated indexes cumulatively, the effect of the number of unpaired electrons becomes evident.

Among the metals considered in this work, the HOMO energy of MnP is markedly higher due to the presence of five unpaired electrons. The electrophilicity of the manganese porphyrin is consistently higher than all of the other porphyrin counterparts irrespective of the conformation of the cation presented to it. It must be recognized that an overall treatment of the complex does not reflect the behavior of the central metal ion and its reducibility. For this reason, we chose to explore the local Fukui indexes on the metal ions, the results of which are presented in the subsequent section.

3.3 Fukui Indices

To probe into the effect of complexation of the imidazolium cation on the porphyrins, the Fukui index was computed taking into consideration the central metal atom (M) and attached pyrrole nitrogens (Npy) for each of them to accommodate the addition of an electron. This was done by altering the electronic state of the $[C_n mim]^+$MP complexes and computing the charges on the metal at both the neutral and electron rich oxidation states. The Fukui index profiles for all of the porphyrin moieties (M+Npy) have been given in Figure 6 as a function of the alkyl chain length in two different conformations. Upon including the pyrrole nitrogens in addition to the central metal ion, the Fukui descriptor for the TU conformations shows that, except for the $[C_2 mim]^+$FeP complex, the Fukui descriptor is negative, indicating the propensity of the metal and pyrrole nitrogen to acquire a fraction of the negative charge added to the complex.

View Article Online
DOI: 10.1039/D5CP02120K

It is noteworthy that all of the other conformations in this homologous series of Fe containing complexes are significantly nucleophilic which posits that both an orbital and conceptual DFT description is required to establish the electron transfer phenomenon. We also note that the Fukui index for electron addition for Fe in case of the $[C_6mim]^+$ bound complex in the TU conformation is considerably higher than the other complexes. This could be tied to the unique geometrical makeup of this complex as compared to the other TU complexes in the same series.[67] In case of this complex, the alkyl chain places itself in a slithered manner to the underlying porphyrin as opposed to pointing away. The local enhancement in the electron density for the porphyrin core seems favorable for all of the 3d metals considered in the work for most of the complexes. A trend for these indices with respect to the alkyl chain length could not be established. However, it is shown that electron addition to the porphyrin is significantly feasible and it is rather necessary imperative to consider the attached pyrrole nitrogens to the central metal ion to evaluate reductive ability of metal porphyrins. The conformations of the cation in complexation play an important role in dictating the local softness of the metal site underneath, which is intuitive as the intermolecular interactions are conformationally dependent. From our earlier analysis concerning electrophilicity of porphyrin, it can also be deduced that local electrophilicity of the metal is quite different as compared to the whole porphyrin. Overall, both the electrophilicity index of the overall porphyrin and the Fukui index of the porphyrin core must be considered for understanding the cumulative effect of the bound cation on the reducibility of the porphyrin.

3.4 NBO Stabilization

For understanding the donor acceptor interaction strength between the cation and the porphyrin, NBO analysis was conducted. The stabilization energies arising from the various orbital interactions between the metal porphyrin as the donor and cation as the acceptor were evaluated. The total stabilization energies computed for both TU and TD conformations for the entire cation space is presented in Figure 7(a) and (b). From the plot concerning TU complexes, it is evident that the

View Article Online
DOI: 10.1039/D5CP02120K

donor-acceptor interactions contribute significantly to the complexes formed between ionic liquid cation and NiP or ZnP. The stabilization energy arising from these interactions does not seem to correlate with the length of the alkyl chain for any of the metals. A similar conclusion can be drawn for the TD conformations except those involving cation-NiP complexes for which the total stabilization energy increases with the alkyl chain length. This trend, however, appears to be nearly absent for other metal porphyrin complexes. To understand the role of the individual monomers in the back-donation process, NBO stabilization energies were resolved further into two donor-acceptor contributions: metal to cation and cation to metal.

Figure 7 (c) and (d) portray the trends in which the metal from the porphyrin macrocycle is considered as the donor while the cation serves as the acceptor. For TU complexes (Figure 7 (c)), energies resulting from these interactions are much more favorable for NiP complexes in comparison other metal complexes, showing that it is one of the key factors leading to the stabilization of the NiP cation complexes. On the other hand, this role of the central porphyrin metal is not pronounced in the case of the other porphyrins. For the TD counterparts, a similar observation can be made in which the Ni component of the metal-cation stabilization energy rises as the alkyl chain is enhanced and the imidazolium ring is displaced from the purview of the porphyrin. Interestingly, the rise in energetic contribution is almost 8 kcal/mol when moving from the $[C_4mim]^+$ to $[C_6mim]^+$ cation while the role of the other metals level off with the increase in size of the cation in the same plot. Thus, it is conceivable that higher donor-acceptor interactions result in increased propensity for ionic liquid cation to bind NiP. Finally, in case where the IL cation in complexation is considered as the donor, the stabilizations are shown in Figures 7 (e) and (f). In Figure 7 (e), the cation shows the greatest energetic stabilizations in case of ZnP, followed by NiP and others in the TU conformation. No such trend can be discerned in case of the TD complexes, in which multiple metal complexes are clustered together. Upon computing the natural charges presented in Tables S6- S11, it is also established that significant charge transfer occurs from the cation to the underlying porphyrin upon binding in case of most of the conformations, comparable to the cases

View Article Online
DOI: 10.1039/D5CP02120K

showing methanol[102] bound to Zn(II) and Mg(II) porphyrins and alkyl ligands bound to Ru(II) porphyrins.[103]

3.5 Core Size

Core size of metal porphyrins is affected by several factors including the presence of axial ligands on either side of the porphyrin plane. In the present work, the cations in complexation with the porphyrins affect the structure and electronic properties of the underlying porphyrins as exhibited by binding energies, DFT indices and stabilization energies. We chose to compare these core sizes for the porphyrins with and without ligand binding. Our calculations for the bare porphyrins agree with the earlier core sizes reported by Kozlowski et al.[104] for these metal porphyrins (Figure 8). In their theoretical treatment of porphyrin core sizes bearing $d^4 - d^{10}$ transition metals, the size of the central cavity was attributed to the occupancy of the electrons in 3d orbital of the central ion (M). Out of these, the configurations of d^5 (all unpaired electrons) and d^{10} (a completely filled shell) for Mn and Zn respectively show the highest core sizes at 2.070 and 2.052 Å respectively. In case of NiP, an empty $d_{x^2-y^2}$ orbital in the ground state leads to the smallest core (1.961 Å) , while the doublet CoP (1.975 Å) falls between NiP and triplet FeP (1.991 Å). The $^3A_{2g}$ structure of FeP is shown to have a core size quite similar to the doublet CuP.

To gauge the effect on the cavity of porphyrins, their core size was examined by calculating the average bond length between the metal and pyrrole nitrogen and taking the difference between the values for the complexes with ionic liquids and bare metal porphyrin. The resulting changes are depicted in Figure 8(a-b). It is clear that the presence of ionic liquids lead to contraction of the underlying porphyrins for most of the TU and TD conformations. The NiP complexes exhibit the largest degree of contraction across both TU and TD conformations. This core contraction could be tied to the stabilization induced metal-cation donor-acceptor interactions, Figure 7(c)). In all of the Zn and Mn bearing porphyrins, a very minimal expansion in the presence of $[C_n\text{mim}]^+$ cations

View Article Online
DOI: 10.1039/D5CP02120K

is observed indicating the two extremes of the 3d electronic occupations. It has been established that a greater core size leads to ease in oxidation[105–107] which is vital for the next step in the cytochrome P-450 cycle where a superoxo ligand sits atop the metal center. Therefore, it is expected that the binding of oxygen may be slightly disfavored for FeP, CoP, NiP, and CuP in comparison to that for the corresponding metal porphyrins. Generally, a relatively larger core aids in an extended π-system promoting electron delocalization amongst the central metal ion and associated pyrrole units. As these core rearrangements cause characteristic changes to the starting symmetry (D_{4h}) of the native unligated planar porphyrins, we decided to examine the vibrational modes and associated distortions of symmetric nature and characterize them according to the motions described in Figure 3.

3.6 Vibrational Analysis

Recently, the effect of symmetry on the tuning of porphyrin properties for tailored reactivity has been studied.[108,109] As the four-fold symmetry of prophyrin is broken due to the presence of ionic liquid cations as ligands, we expect that the redox potential of the underlying porphyrin is affected as already demonstrated through the electrophilicity index calculation. In order to quantify the structural alteration in porphyrins, normal modes of the vibrations for the optimized geometries were analyzed for each set of conformations for every porphyrin included in the work. For probing the substrate binding effects, only the out-of-plane (OOP) modes were recorded. The five different motions affecting the size of the central porphyrin cavity and OOP displacements are saddling, ruffling, doming, waving, and propellering. These motions are pictured in Figure 3 for NiP. In the review on structural significance of porphyrins by Kingsbury and Senge,[99] for the out of plane normal modes, B_{2u} and B_{1u} correspond to saddling and ruffling, A_{2u} to doming, $E_{g(x)}$ and $E_{g(y)}$ to waving, and finally A_{1u} to propellering. While both ruffling and saddling act as driving force for generating D_{2d} symmetric structures, doming corresponds to C_{4v} while the orthogonally complementary waving motions present a C_{2h} symmetry. In case of saddling, the six atoms within each pyrrole ring are subdivided such that they undergo motions in the upward and downward direc-

View Article Online
DOI: 10.1039/D5CP02120K

tions equally. Ruffling, on the other hand, is caused by the complementary motion of adjacent pyrroles moving in opposite directions. Both saddling and ruffling cause the electron rich cavity of porphyrin to contract whereas doming causes it to expand. For doming, the pyrroles all move in a concerted manner to increase the strain on the outer porphyrin skeleton, thereby increasing the cavity size.

The modes for all of these representative motions are presented for both the TU and TD conformations of cations bound to the underlying porphyrin and the out-of-plane distortions induced by each of these modes are collected in the Supporting Information (Tables S12 - S23) Figure 8(c) gives an average treatment of the out-of-plane displacements (D_{OOP}) arising in the porphyrin skeletons in complex with the cation in both TU and TD conformations. This was computed taking into consideration the D_{4h} symmetry of the porphyrin macrocycle and that the associated distortions would be distributed among the normal modes arising due to presence of cation. D_{OOP} values indicate that the effect of cations on the distortions is minimal for MnP and ZnP, irrespective of the type of conformations presented to porphyrins, while the highest distortions $>$ 1Å are observed for NiP. The other three metalloporphyrins (FeP, CoP, CuP) exhibit intermediate values of D_{OOP} - in the range of 0.4-0.6 Å. Some of the common observations in case of all of the vibrational modes is the predominance of saddling (B_{2u}) and ruffling (B_{1u}) motions for most of the porphyrins. For Zn and Mn containing complexes, significant doming effect (A2u) is also observed for some of the TD conformations. Also, the propellering effect of the A_{1u} is mostly negligible as compared to the rest of the out of plane symmetry modes in case of most of the $[C_n\mathrm{mim}]^+$ MP complexes.

From the initial analyses, it can be ascertained that while the magnitude of doming and waving effects are distributed, saddling and ruffling constitute majority of the overall |Doop| displacement reported for each set of $[C_n\mathrm{mim}]^+$ MP complexes. The D_{2d} symmetry type is preferred over the initial D_{4h} one in the case of most of the metal complexes. Irrespective of the conformation presented, these two modes show the highest contributions to the out of plane normal deformations that is also representative of the contraction of the porphyrin cavity (Figure 8). Both Mn and Zn

View Article Online
DOI: 10.1039/D5CP02120K

containing complexes, however, show a greater doming character as compared to the other metal porphyrins, rather exhibiting expansion of the same cavity. Interestingly, these two porphyrins are also the ones that contain the highest and the lowest number of unpaired electrons (five for MnP and none for ZnP).

View Article Online
DOI: 10.1039/D5CP02120K

4 Conclusion

The present work is an extension of our former work concerning the complexation of the iron porphyrins with 1-n-alkyl-3-methylimidazolium cations to understanding their binding through electronic and geometrical peorperties. We considered six different porphyrins containing different metal centers, namely, Iron (Fe), Nickel (Ni), Zinc (Zn), Cobalt (Co), Copper (Cu) and Manganese (Mn). The binding of these porphyrins to two different conformations, tail up (TU) and tail down (TD) of the imidazolium-based cations have been studied. Results show a conformational dependence on the binding affinity as the alkyl chain on the cation is enhanced similar to the observation made by us in case of iron porphyrin. Upon evaluating the electrophilicity indexes, it was shown that similar to FeP complexes formerly, elevated reactivity is shown in case of all of the cation bound metal porphyrins. In order to further understand the role of the cations the reducibility of the porphyrin, Fukui indices were evaluated on these optimized complexes. The Fukui analysis provided insight into the role of the porphyrin core in the overall reducibility of the metal porphyrins. Both electrophilicity and local charge differences are required to analyze the electron addition to ligated porphyrins. The NBO analysis exhibited that the Lewis interactions between the possible donor acceptor combinations is most favorable for the singlet Nickel and Zinc complexes while for the others, the second order stabilizations cannot be distinguished. Our core size analysis of the porphyrins also sheds light on the contraction of the porphyrin cavity for NiP complexes. The motions of saddling, ruffling and doming are observed to govern the shape of the porphyrin cavity. Porphyrins having a native D_{4h} symmetry, when bound to $[C_n\text{mim}]^+$ cations revert to the D_{2h} symmetric form but in the case of Mn and Zn, there is significant doming character in addition to the B_{2u} and B_{1u} modes showing highest displacement, owing to a larger cavity as compared to others. These cavity effects are important in the scheme of the overall catalytic cycle, expected to influence proton addition in subsequent steps.

View Article Online
DOI: 10.1039/D5CP02120K

5 Tables

Table 1: Relative Spin State Energetics for the metal porphyrins considered in the present work. The most stable spin state is recorded in bold.

MP	Index	Spin State	Relative Energy (kcal/mol)
Mn	MP_1	$^2MP_1(^4MP_1)(\mathbf{^6MP_1})$	(63.1)(11.4)**(0.0)**
Fe	MP_1	$^1MP_2$ $(\mathbf{^3MP_2})(^5MP_2)$	(39.4)**(0.0)**(6.4)
Co	MP_3	$\mathbf{^2MP_3}$ $(^4MP_3)(^6MP_3)$	**(0.0)**(12.4)(45.2)
Ni	MP_4	$\mathbf{^1MP_4}(^3MP_4)(^5MP_4)$	**(0.0)**(16.2)(58.2)
Cu	MP_5	$\mathbf{^2MP_5}(^4MP_5)(^6MP_5)$	**(0.0)**(41.2)(84.3)
Zn	MP_6	$\mathbf{^1MP_6}(^3MP_6)(^5MP_6)$	**(0.0)**(43.1)(82.9)

Table 2: Relative binding energies of $[C_n mim]^+$-MP complexes (kcal/mol) for tail up (TU) and tail down (TD) conformations of bound $[C_n mim]^+$ cations

Cation	Mn		Fe		Co		Ni		Cu		Zn	
	TU	TD	TU	TD	TU	TD	TU	TD	TU	TD	TU	TD
$[C_2mim]^+$	0.0	0.0	0.7	0.0	0.4	0.0	0.7	0.0	0.0	0.7	0.0	1.3
$[C_4mim]^+$	0.0	0.2	1.1	0.0	0.1	0.0	1.1	0.0	0.9	0.0	0.0	0.5
$[C_6mim]^+$	0.0	1.4	0.0	1.0	0.0	0.1	0.0	1.7	0.0	1.5	0.0	3.6
$[C_8mim]^+$	0.0	2.8	0.0	2.8	0.0	3.4	0.0	1.8	0.0	1.8	0.0	2.2
$[C_{10}mim]^+$	0.0	2.9	0.0	3.1	0.0	2.7	0.0	2.6	0.0	2.4	0.0	2.3

View Article Online
DOI: 10.1039/D5CP02120K

Table 3: Global relative binding energies of $[C_n mim]^+$-MP complexes (kcal/mol) for tail up (TU) and tail down (TD) conformations of bound $[C_n mim]^+$ cations

Cation	TU						TD					
	Mn	Fe	Co	Ni	Cu	Zn	Mn	Fe	Co	Ni	Cu	Zn
$[C_2mim]^+$	1.0	1.2	0.9	0.0	1.3	2.7	1.7	1.3	1.2	0.0	2.7	4.7
$[C_4mim]^+$	1.1	0.6	0.8	0.0	2.0	3.0	2.3	2.0	1.9	0.0	2.2	4.6
$[C_6mim]^+$	1.0	0.1	2.2	0.0	2.0	2.3	1.2	0.0	1.1	0.5	2.3	4.7
$[C_8mim]^+$	1.0	0.6	1.0	0.0	2.2	2.6	2.0	1.5	2.5	0.0	2.2	2.9
$[C_{10}mim]^+$	1.0	0.7	0.8	0.0	2.2	2.6	1.3	1.2	0.9	0.0	2.0	2.3

View Article Online
DOI: 10.1039/D5CP02120K

6 Figures

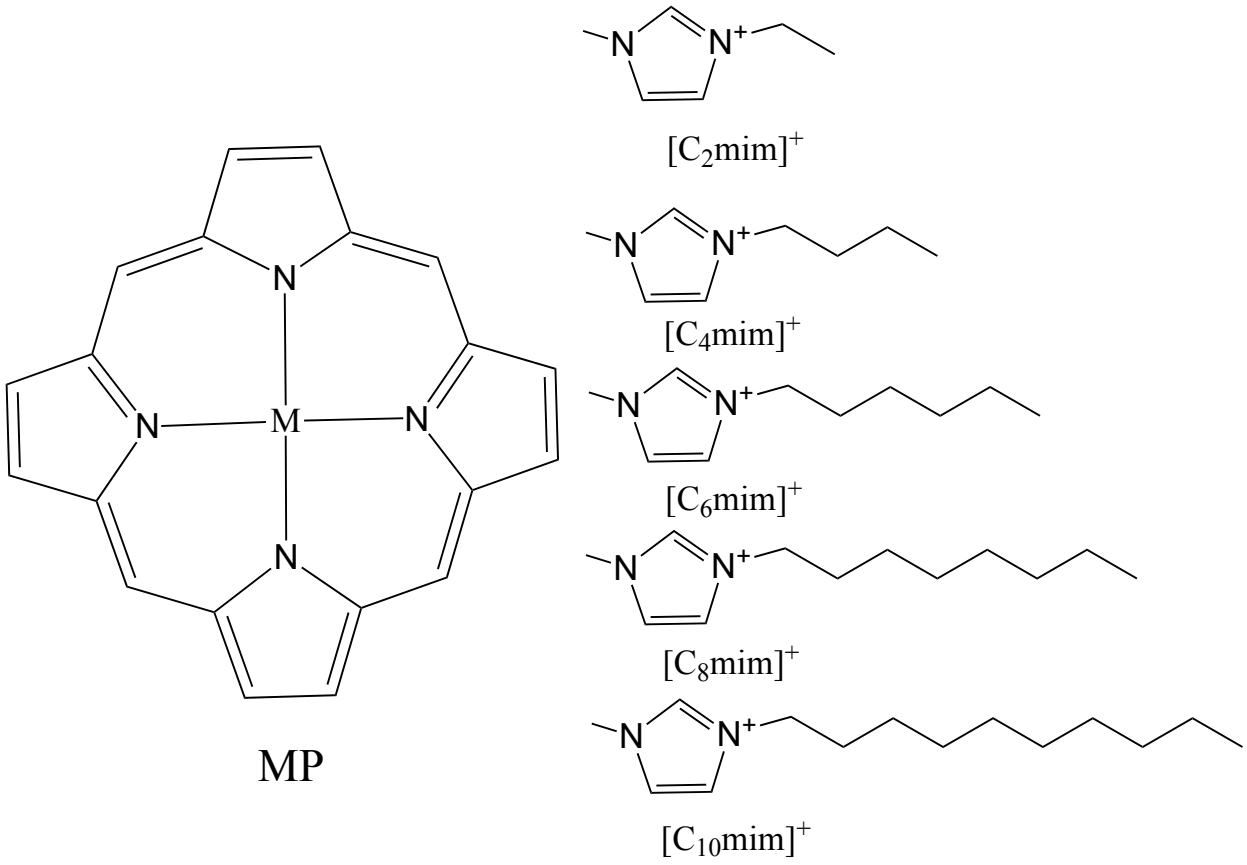

Figure 1: Schematic showing the system considered for performing DFT calculations (Metal Porphyrin (MP) and 1-n-alkyl-3-methylimidazolium cation ($[C_n mim]^+$)

View Article Online
DOI: 10.1039/D5CP02120K

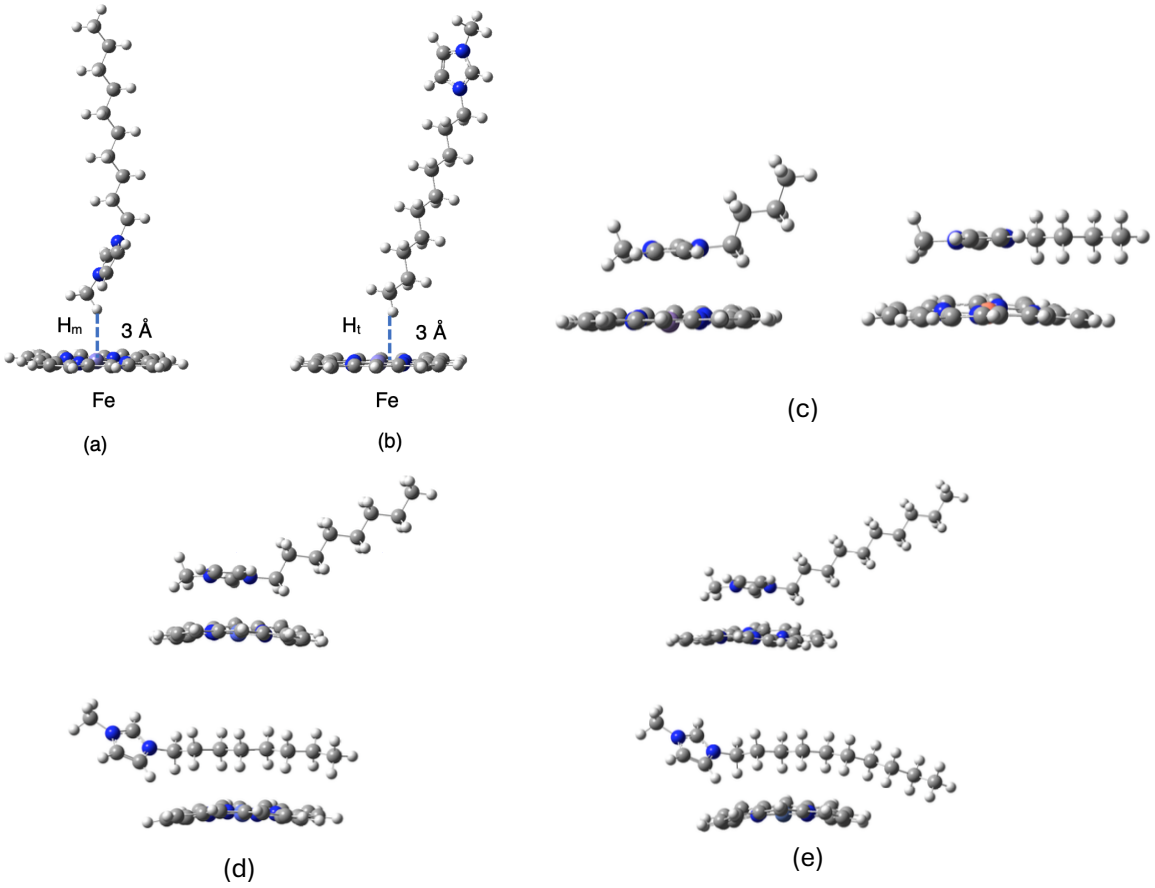

Figure 2: Initial conformations for optimization of (a) Tail Up (TU) and (b) Tail Down (TD) structures shown for a $[C_n mim]^+$FeP system : H_m - methyl hydrogen facing the metal ion, H_t - terminal alkyl chain hydrogen facing the metal ion, optimized geometries of (c) $[C_4 mim]^+$MnP TU and TD (d) $[C_8 mim]^+$CoP TU and TD (e) $[C_{10} mim]^+$NiP TU and TD complexes

View Article Online
DOI: 10.1039/D5CP02120K

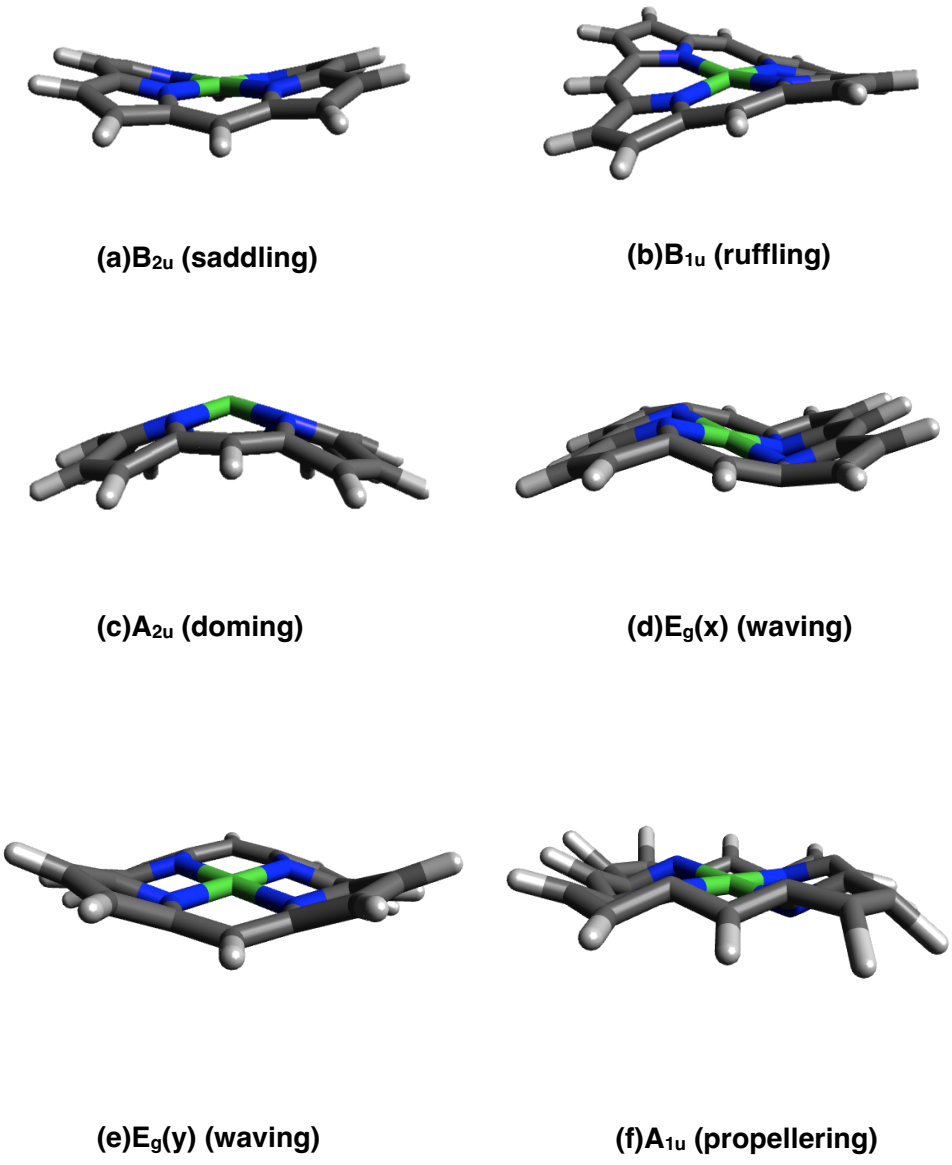

Figure 3: Schematic showing deformation characteristics of the out-of-plane normal modes for nickel porphyrin (in stick models); color coding - white : Hydrogen, gray : Carbon, blue : Nitrogen, green : Nickel

View Article Online
DOI: 10.1039/D5CP02120K

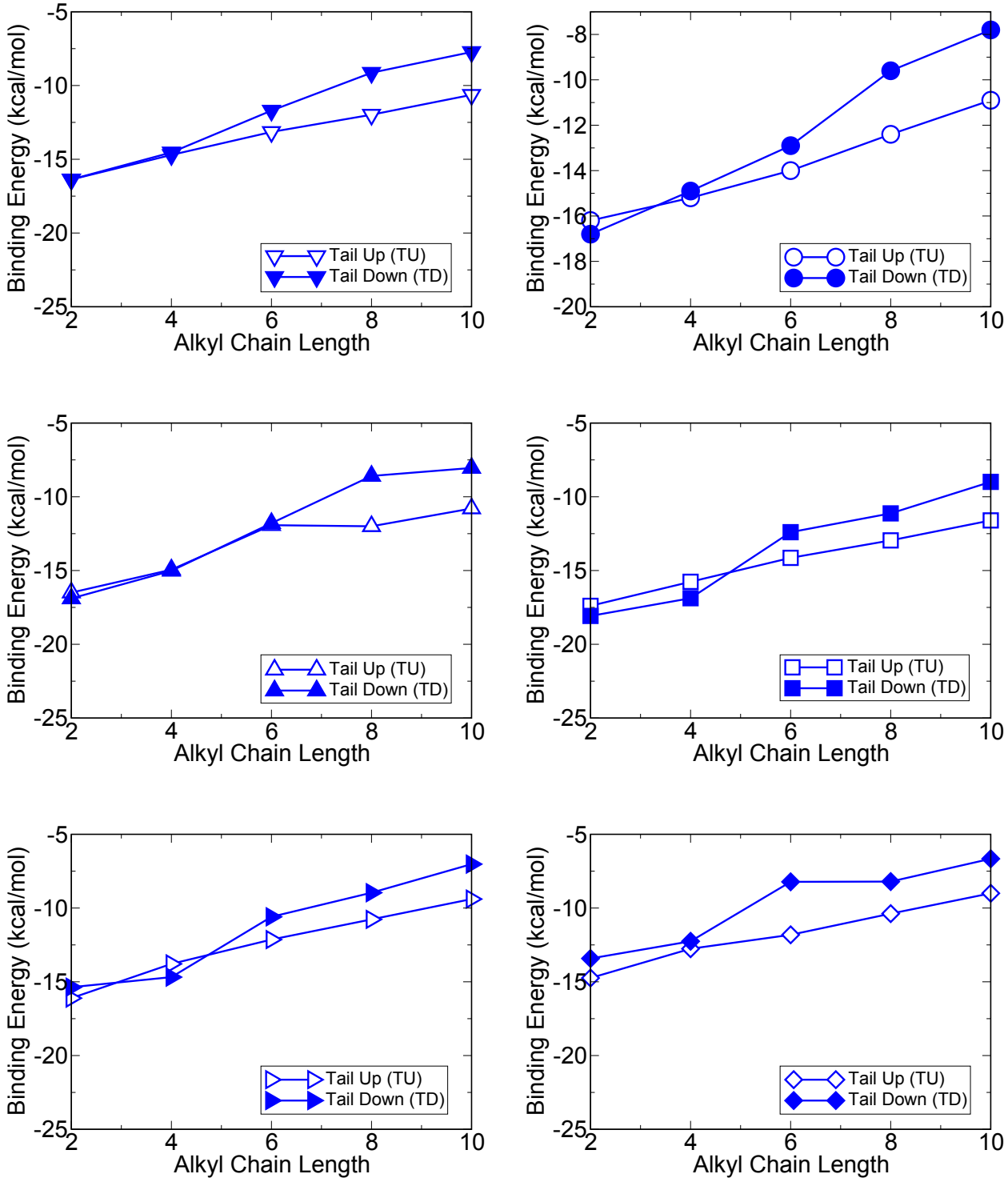

(e) M = Cu (f) M = Zn

Figure 4: Binding energy profiles for metal porphyrin cation complexes ($[C_n mim]^+$MP) M is (a) Mn ▽ (b) Fe ○ (c) Co △ (d) Ni □ (e) Cu ▷ (f) Zn ◊ ; unfilled symbols (TU) , filled symbols (TD)

View Article Online
DOI: 10.1039/D5CP02120K

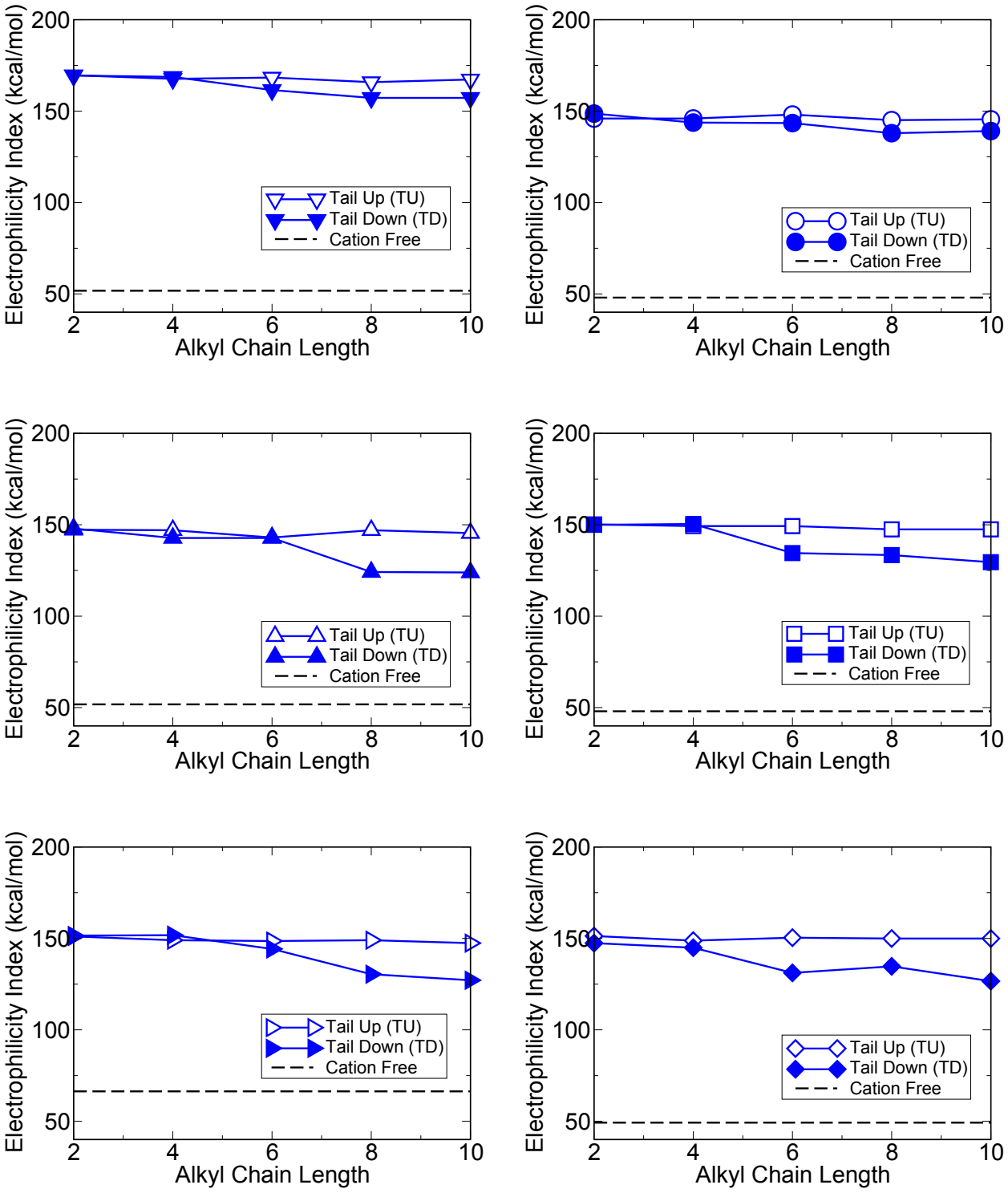

(e) M = Cu (f) M = Zn

Figure 5: Electrophilicity indexes for metal porphyrin cation complexes (MP$[C_n mim]^+$) M is (a) Mn ▽ (b) Fe ○ (c) Co △ (d) Ni □ (e) Cu ▷ (f) Zn ◊ ; unfilled symbols (TU), filled symbols (TD)

View Article Online
DOI: 10.1039/D5CP02120K

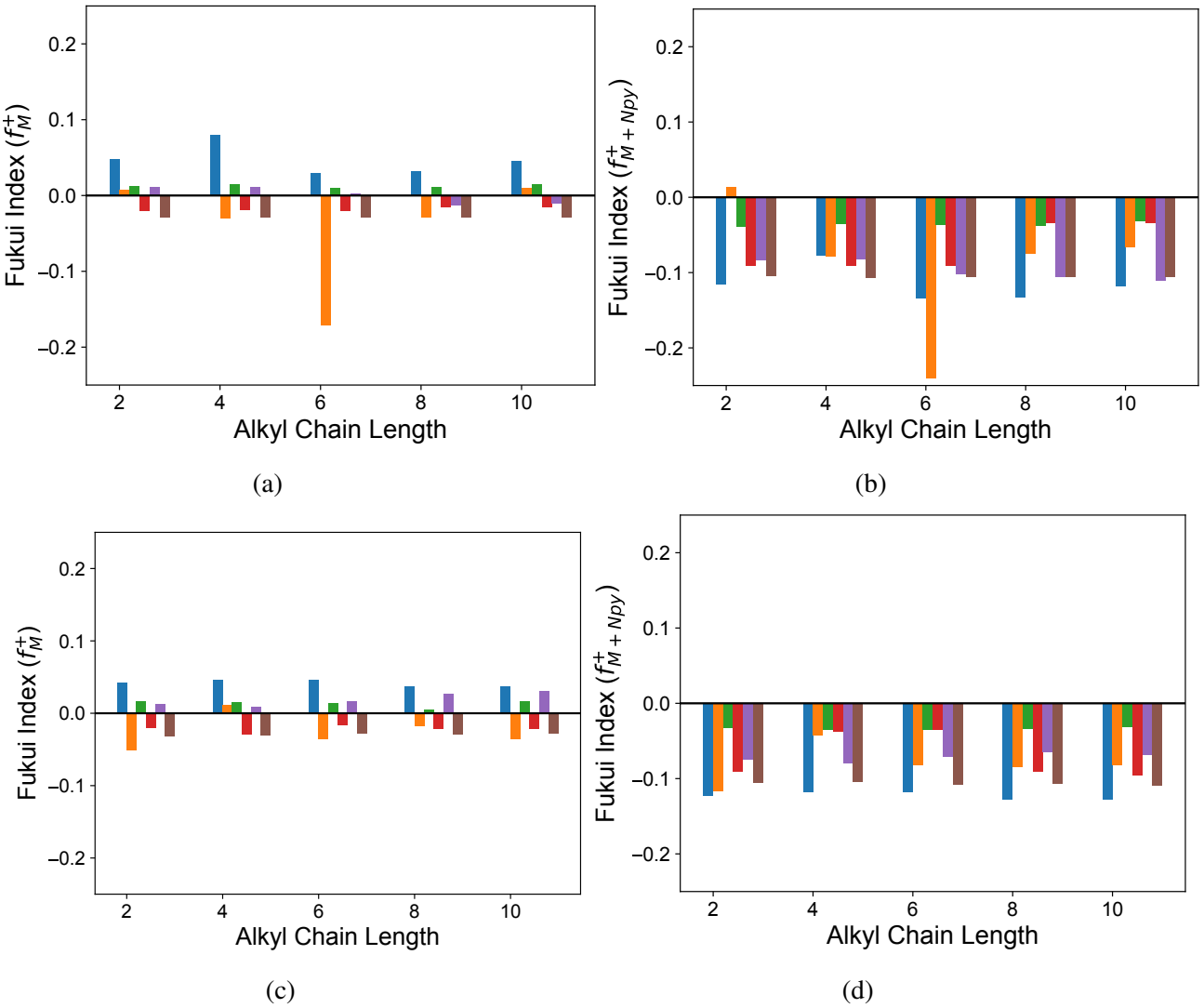

Figure 6: Fukui index for addition of electron to the porphyrin metal (f_M^+) in TU (a) and TD (c) conformations and including pyrrole nitrogens (f_{M+Npy}^+) for (b) TU (d) TD conformations. color coding : Mn (blue), Fe (orange), Co (green), Ni (red), Cu (purple), Zn (brown)

View Article Online
DOI: 10.1039/D5CP02120K

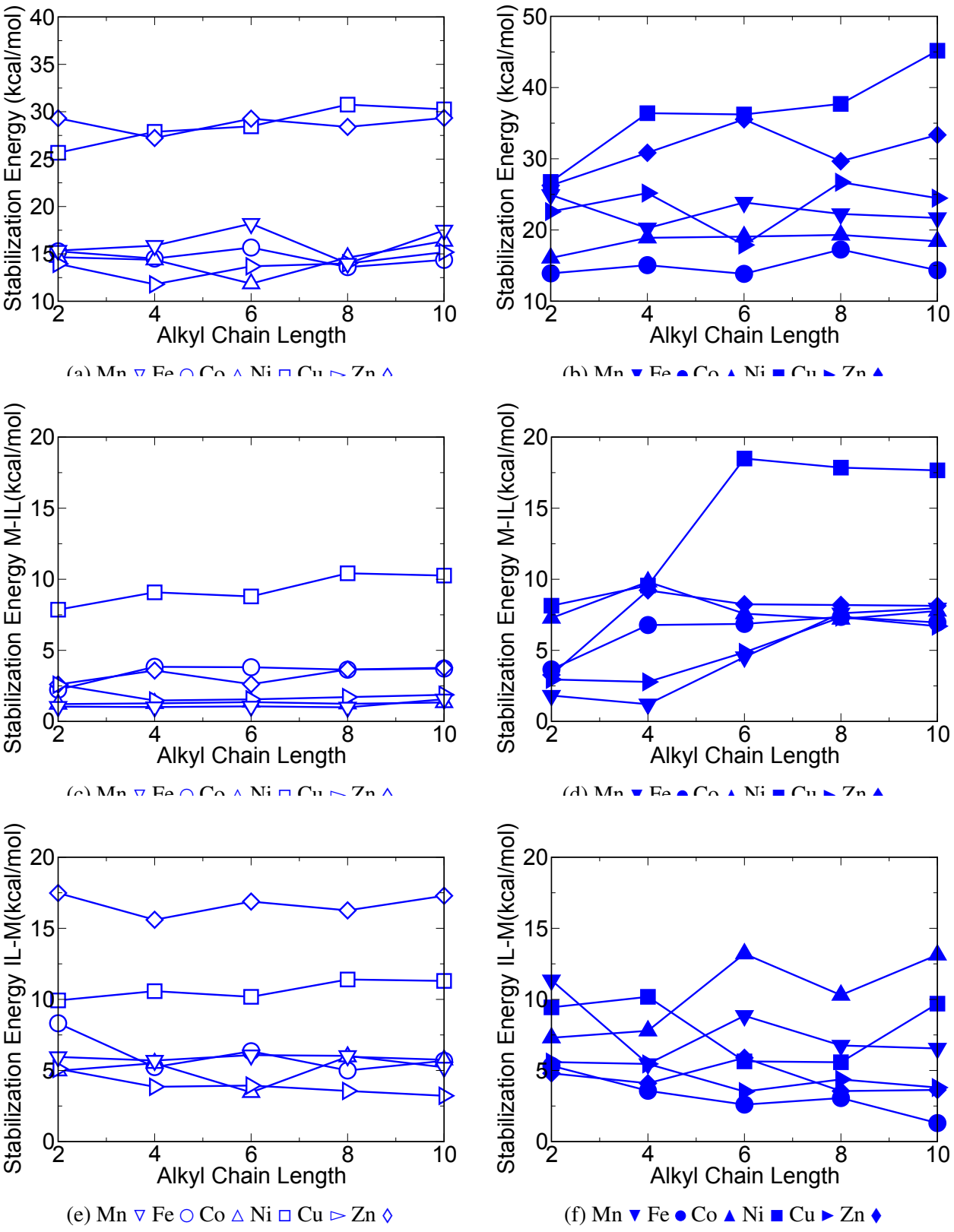

Figure 7: NBO stabilization for cation metal porphyrin complexes (a) TU combined (c) TU metal to cation (M-IL) (e) TU cation to metal (IL-M), (b) TD combined (d) TD metal to cation (M-IL) (f) TD cation to metal (IL-M) ; unfilled symbols (TU) , filled symbols (TD).

View Article Online
DOI: 10.1039/D5CP02120K

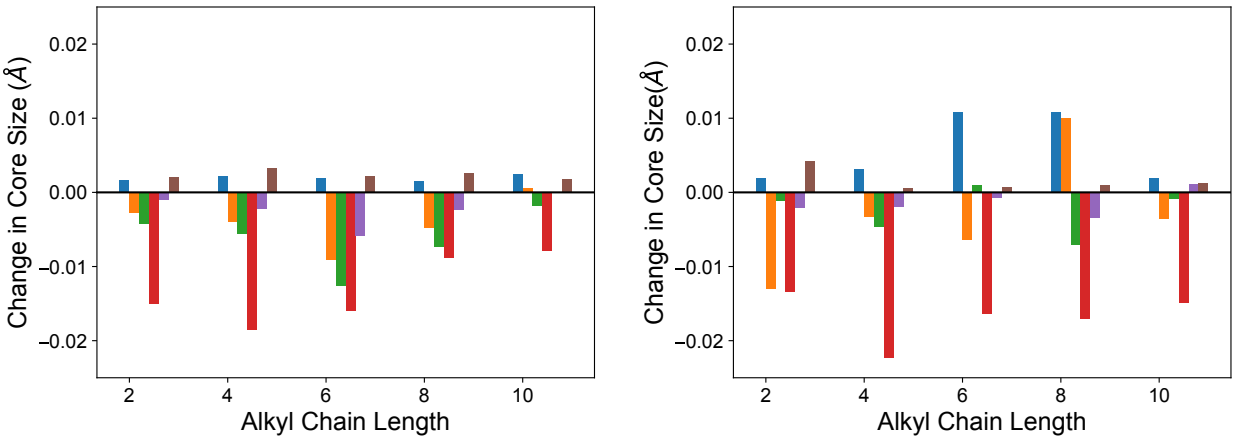

(a)

(b)

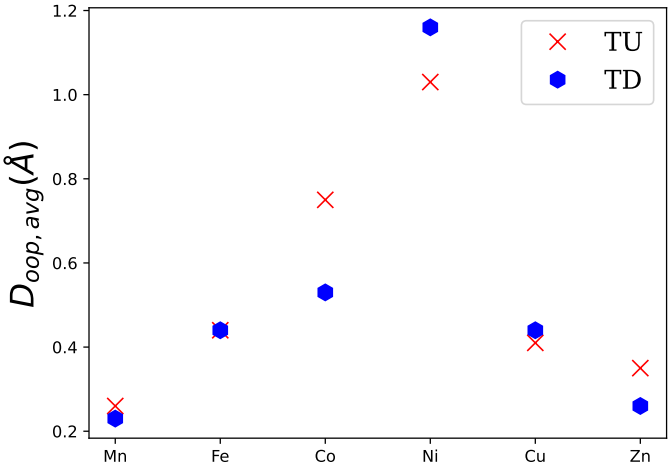

(c)

Figure 8: Core size change for metal porphyrins in (a) TU (b) TD conformations upon exposure to $[C_n mim]^+$ cations, color coding : Mn (blue) , Fe (orange), Co (green), Ni (red), Cu (purple), Zn (brown). (c) Average out-of-plane deformations from first six normal modes for all of the porphyrin skeletons in TU and TD conformations calculated from displacements recorded for cation chain lengths 2-10.

View Article Online
DOI: 10.1039/D5CP02120K

Acknowledgments

The authors gratefully acknowledge the funding provided by the National Science Foundation (Grant No. CBET-1845143). The computing for this project was performed at the OSU High Performance Computing Center at Oklahoma State University, which was supported, in part, by the National Science Foundation (Grant No. OAC-1531128).

Supporting Information Available

Side view of the optimized geometries of the cation metal porphyrin complexes, associated vibrational modes, their 3d representation, and out-of-plane normal mode displacements are provided in the supplementary information.

References

(1) Wang, P.; Zakeeruddin, S.; Moser, J.; Gradtzel, M. A New Ionic Liquid Electrolyte Enhances the Conversion Efficiency of Dye-Sensitized Solar Cells. *J. Phys. Chem. B* **2003**, *107*, 13280–13285.

(2) Wasserscheid, P.; Keim, W. Ionic Liquids - New Solutions for Transition Metal Catalysis. *Angew. Chem. Int. Ed.* **2000**, *39*, 3772–3789.

(3) Szymczak, J.; Legeai, S.; Michel, S.; Diliberto, S.; Stein, N.; Boulanger, C. Electrodeposition of Stoichiometric Bismuth Telluride Bi_2Te_3 Using a Piperidinium Ionic Liquid Binary Mixture. *Electrochim. Acta* **2014**, *137*, 586–594.

(4) Liu, Z.; Cui, T.; Lu, T.; Shapouri Ghazvini, M.; Endres, F. Anion Effects on the Solid/Ionic Liquid Interface and the Electrodeposition of Zinc. *J. Phys. Chem. C* **2016**, *120*, 20224–20231.

View Article Online
DOI: 10.1039/D5CP02120K

(5) Pino, V.; Afonso, A. M. Surface-Bonded Ionic Liquid Stationary Phases in High-Performance Liquid Chromatography–A Review. *Anal. Chim. Acta* **2012**, *714*, 20–37.

(6) Liu, J.; Jiang, G.; Jaunsson, J. A. Application of Ionic Liquids in Analytical Chemistry. *Trends in Anal. Chem.* **2005**, *24*, 20–27.

(7) Anthony, J. L.; Maginn, E. J.; Brennecke, J. F. Solubilities and Thermodynamic Properties of Gases in the Ionic Liquid 1-n-Butyl-3-Methylimidazolium Hexafluorophosphate. *J. Phys. Chem. B* **2002**, *106*, 7315–7320.

(8) Lei, Z.; Dai, C.; Chen, B. Gas Solubility in Ionic Liquids. *Chem. Rev.* **2014**, *114*, 1289–1326.

(9) Bara, J. E.; Carlisle, T. K.; Gabriel, C. J.; Camper, D.; Finotello, A.; Gin, D. L.; Noble, R. D. Guide to CO_2 Separations in Imidazolium-Based Room-Temperature Ionic Liquids. *Ind. Eng. Chem. Res.* **2009**, *48*, 2739–2751.

(10) Almantariotis, D.; Stevanovic, S.; Fandiso, O.; Pensado, A. S.; Padua, A. A. H.; Coxam, J. Y.; Costa Gomes, M. F. Absorption of Carbon Dioxide, Nitrous Oxide, Ethane and Nitrogen by 1-Alkyl-3-Methylimidazolium ($[C_n mim]^+$, n= 2,4,6) Tris(Pentafluoroethyl)Trifluorophosphate Ionic Liquids (eFAP). *J. Phys. Chem. B* **2012**, *116*, 7728–7738.

(11) Bidikoudi, M.; Stergiopoulos, T.; Likodimos, V.; Romanos, G. E.; Francisco, M.; Iliev, B.; Adamova, G.; Schubert, T. J. S.; Falaras, P. Ionic Liquid Redox Electrolytes based on Binary Mixtures of 1-Alkyl-Methylimidazolium Tricyanomethanide with 1-Methyl-3-Propylimidazolium Iodide and Implication in Dye-Sensitized Solar Cells. *J. Mater. Chem. A* **2013**, *1*, 10474–10486.

(12) Pinilla, C.; Del Popolo, M.; Lynden-Bell, R.; Kohanoff, J. Structure and Dynamics of a Confined Ionic Liquid. Topics of Relevance to Dye-Sensitized Solar Cells. *J. Phys. Chem. B* **2005**, *109*, 17922–17927.

View Article Online
DOI: 10.1039/D5CP02120K

(13) Lane, G. H.; Bayley, P. M.; Clare, B. R.; Best, A. S.; Macfarlane, D. R.; Forsyth, M.; Hollenkamp, A. F. Ionic Liquid Electrolyte for Lithium Metal Batteries: Physical, Electrochemical, and Interfacial Studies of N-Methyl-N-Butylmorpholinium Bis(Fluorosulfonyl)Imide. *J. Phys. Chem. C* **2010**, *114*, 21775–21785.

(14) Basile, A.; Yoon, H.; MacFarlane, D. R.; Forsyth, M.; Howlett, P. C. Investigating Non-Fluorinated Anions for Sodium Battery Electrolytes Based on Ionic Liquids. *Electrochem. Comm.* **2016**, *71*, 1–14.

(15) Costa, L. T.; Sun, B.; Jeschull, F.; Brandell, D. Polymer-Ionic Liquid Ternary Systems for Li-Battery Electrolytes: Molecular Dynamics Studies of LiTFSI in a $[Emim]^+$-TFSI and PEO Blend. *J. Chem. Phys.* **2015**, *143*, 1–10.

(16) Chatel, G.; Pereira, J.; Debbeti, V.; Wang, H.; Rogers, R. D. Mixing Ionic Liquids – "Simple Mixtures" or "Double Salts"? *Green Chem.* **2014**, *16*, 2051–2133.

(17) Fillion, J. J.; Brennecke, J. F. Viscosity of Ionic Liquid–Ionic Liquid Mixtures. *J. Chem. Eng. Data* **2017**, *62*, 1884–1901.

(18) Aparicio, S.; Atilhan, M. Mixed Ionic Liquids: The Case of Pyridinium-Based Fluids. *J. Phys. Chem. B* **2012**, *116*, 2526–2537.

(19) García, G.; Atilhan, M.; Aparicio, S. Interfacial Properties of Double Salt Ionic Liquids: A Molecular Dynamics Study. *J. Phys. Chem. C* **2015**, *119*, 28405–28416.

(20) Shimizu, K.; Tariq, M.; Gomes, M. F. C.; Rebelo, L.; Canongia Lopes, J. Assessing the Dispersive and Electrostatic Components of the Cohesive Energy of Ionic Liquids Using Molecular Dynamics Simulations and Molar Refraction Data. *J. Phys. Chem. B* **2010**, *114*, 5831–5834.

(21) Payal, R. S.; Balasubramanian, S. Homogenous Mixing of Ionic Liquids: Molecular Dynamics Simulations. *Phys. Chem. Chem. Phys.* **2013**, *15*, 21077–21083.

View Article Online
DOI: 10.1039/D5CP02120K

(22) Almeida, H. F. D.; Lopes, J. N. C.; Rebelo, L. P. N.; Coutinho, J. A. P.; Freire, M. G.; Marrucho, I. M. Densities and Viscosities of Mixtures of Two Ionic Liquids Containing a Common Cation. *J. Chem. Eng. Data* **2016**, 10.1021/acs.jced.6b00178.

(23) Wasserscheid, P., Welton, T., Eds. *Ionic Liquids in Synthesis*; 2005.

(24) Zhang, Y.; Bakshi, B. R.; Demessie, E. S. Life Cycle Assessment of an Ionic Liquid Versus Molecular Solvents and their Applications. *Environ. Sci. & Technol.* **2008**, *42*, 1724–1730.

(25) Ma, J. W.; Zhou, Z.; Zhang, F.; Fang, C. G.; Wu, Y. T.; Zhang, Z. B.; Li, A. M. Ditetraalkylammonium Amino Acid Ionic Liquids as CO_2 Absorbents of High Capacity. *Environ. Sci. & Technol.* **2011**, *45*, 10627–10633.

(26) Docherty, K. M.; Young, K. C.; Maurice, P. A.; Bridgham, S. D. Dissolved Organic Matter Concentration and Quality Influences upon Structure and Function of Freshwater Microbial Communities. *Microb. Ecol.* **2006**, *52*, 378–388.

(27) Oskarsson, A.; Wright, M. C. Ionic Liquids: New Emerging Pollutants, Similarities with Perfluorinated Alkyl Substances (PFASs). *Environ. Sci. & Technol.* **2019**, *53*, 10539–10541.

(28) Mehrkesh, A.; Karunanithi, A. T. Life-Cycle Perspectives on Aquatic Ecotoxicity of Common Ionic Liquids. *Environ. Sci. & Technol.* **2016**, *50*, 6814–6821.

(29) Abai, M.; Atkins, M. P.; Hassan, A.; Holbrey, J. D.; Kuah, Y.; Nockemann, P.; Oliferenko, A. A.; Plechkova, N. V.; Rafeen, S.; Rahman, A. A. et al. An Ionic Liquid Process for Mercury Removal From Natural Gas. *Dalton Trans.* **2015**, *44*, 8617–8624.

(30) Han, X.; Scott, A. C.; Fedorak, P. M.; Bataineh, M.; Martin, J. W. Influence of Molecular Structure on the Biodegradability of Naphthenic Acids. *Environ. Sci. & Technol.* **2008**, *42*, 1290–1295.

View Article Online
DOI: 10.1039/D5CP02120K

(31) Misiti, T. M.; Tezel, U.; Pavlostathis, S. G. Effect of Alkyl Side Chain Location and Cyclicity on the Aerobic Biotransformation of Naphthenic Acids. *Environ. Sci. & Technol.* **2014**, *48*, 7909–7917.

(32) Wijker, R. S.; Kurt, Z.; Spain, J. C.; Bolotin, J.; Zeyer, J.; Hofstetter, T. B. Isotope Fractionation Associated with the Biodegradation of 2- and 4-nitrophenols via Monooxygenation Pathways. *Environ. Sci. & Technol.* **2013**, *47*, 14185–14193.

(33) Docherty, K. M.; Joyce, M. V.; Kulacki, K. J.; Kulpa, C. F. Microbial Biodegradation and Metabolite Toxicity of Three Pyridinium-based Cation Ionic Liquids. *Green Chem.* **2010**, *12*, 701–712.

(34) Gathergood, N.; Garcia, M. T.; Scammells, P. J. Biodegradable Ionic Liquids: Part I. Concept, Preliminary Targets and Evaluation. *Green Chem.* **2004**, *6*, 166–175.

(35) Markiewicz, M.; Jungnickel, C.; Cho, C.; Stolte, S. Mobility and Biodegradability of an Imidazolium-based Ionic Liquid in Soil and Soil Amended with Waste-sewage Sludge. *Environ. Sci.: Processes and Impacts* **2015**, *17*, 1462–1469.

(36) Docherty, K. M.; Aiello, S. W.; Buehler, B. K.; Jones, S. E.; Szymczyna, K. A., B. R.and Walker Ionic Liquid Biodegradability Depends on Specific Wastewater Microbial Consortia. *Chemosphere* **2015**, *136*, 160–166.

(37) Romero, A.; Santos, A.; Tojo, J.; Rodriguez, A. Toxicity and Biodegradability of Imidazolium Ionic Liquids. *J. Hazard. Mater.* **2008**, *151*, 268–273.

(38) Ford, L.; Harjani, J. R.; Atefi, F.; Garcia, M. T.; Singer, R. D.; Scammells, P. J. Further Studies on the Biodegradation of Ionic Liquids. *Green Chem.* **2010**, *12*, 1783–1789.

(39) Neumann, J.; Steudte, S.; Cho, C.-W.; Thöming, J.; Stolte, S. Biodegradability of 27 Pyrrolidinium, Morpholinium, Piperidinium, Imidazolium and Pyridinium Ionic Liquid Cations Under Aerobic Conditions. **2014**, *16*, 2174–2184.

View Article Online
DOI: 10.1039/D5CP02120K

(40) Docherty, K. M.; Dixon, J. K.; Kulpa Jr, C. F. Biodegradability of Imidazolium and Pyridinium Ionic Liquids by an Activated Sludge Microbial Community. *Biodegradation* **2007**, *18*, 481–493.

(41) Stolte, S.; Steudte, S.; Igartua, A.; Stepnowski, P. The Biodegradation of Ionic Liquids - the View from a Chemical Structure Perspective. *Curr. Org. Chem.* **2011**, *15*, 1946–1973.

(42) Jordan, A.; Gathergood, N. Biodegradation of ionic liquids – a critical review. *Chem. Soc. Rev.* **2015**, *44*, 8200–8237.

(43) Petkovic, M.; Seddon, K. R.; Rebelo, L. P. N.; Pereira, C. S. Ionic liquids: A Pathway to Environmental Acceptability. *Chem. Soc. Rev.* **2011**, *40*, 1383–1403.

(44) Coleman, D.; Gathergood, N. Biodegradation Studies of Ionic Liquids. *Chem. Soc. Rev.* **2010**, *39*, 600–637.

(45) Gathergood, N.; Scammells, P. J.; Garcia, M. T. Biodegradable ionic liquids : Part III. The first readily biodegradable ionic liquids. *Green Chem.* **2006**, *8*, 156–160.

(46) Garcia, M. T.; Gathergood, N.; Scammells, P. J. Biodegradable ionic liquids Part II. Effect of the Anion and Toxicology. *Green Chem.* **2005**, *7*, 9–14.

(47) Stepnowski, P.; Mrozik, W.; Nichthauser, J. Adsorption of Alkylimidazolium and Alkylpyridinium Ionic Liquids onto Natural Soils. *Environ. Sci. & Technol.* **2007**, *41*, 511–516.

(48) Siedlecka, E. M.; Stepnowski, P. The Effect of Alkyl Chain Length on the Degradation of Alkylimidazolium and Pyridinium-type Ionic Liquids in a Fenton-like System. *Environ. Sci. Pollut. Res.* **2008**, *16*, 453–458.

(49) Stepnowski, P.; Storoniak, P. Lipophilicity and Metabolic Route Prediction of Imidazolium Ionic Liquids. *Environ. Sci. Pollut. Res.* **2005**, *12*, 199–204.

View Article Online
DOI: 10.1039/D5CP02120K

(50) Pham, T. P. T.; Cho, C. W.; Jeon, C. O.; Chung, Y. J.; Lee, M. W.; Yun, Y. S. Identification of Metabolites Involved in the Biodegradation of the Ionic Liquid 1-butyl-3-methylpyridinium bromide by Activated Sludge Microorganisms. *Environ. Sci. & Technol.* **2009**, *43*, 516–521.

(51) Stolte, S.; Abdulkarim, S.; Arning, J.; Blomeyer-Nienstedt, A.-K.; Bottin-Weber, U.; Matzke, M.; Ranke, J.; Jastorff, B.; Thöming, J. Primary Biodegradation of Ionic Liquid Cations, Identification of Degradation Products of 1-methyl-3-octylimidazolium chloride and Electrochemical Wastewater Treatment of Poorly Biodegradable Compounds. *Green Chem.* **2008**, *10*, 214–224.

(52) Pham, T. P. T.; Cho, C. W.; Yun, Y. S. Environmental Fate and Toxicity of Ionic Liquids: A Review. *Water Res.* **2010**, *44*, 352–372.

(53) Pham, T. P. T.; Cho, C.-W.; Yun, Y.-S. Structural Effects of Ionic Liquids on Microalgal Growth Inhibition and Microbial Degradation. *Environ. Sci. Pollut. Res.* **2016**, 1–7.

(54) Zhang, C.; Wang, H.; Malhotra, S. V.; Dodge, C. J.; Francis, A. J. Biodegradation of Pyridinium-based Ionic Liquids by an Axenic Culture of Soil *Corynebacteria*. *Green Chem.* **2010**, *12*, 851–858.

(55) Guengerich, F. P.; Munro, A. W. Unusual Cytochrome P450 Enzymes and Reactions. *J. Biol. Chem.* **2013**, *288*, 17065–17073.

(56) Guengerich, F. P.; Sohl, C. D.; Chowdhury, G. Multi-step Oxidations Catalyzed by Cytochrome P450 Enzymes: Processive vs. Distributive Kinetics and the Issue of Carbonyl Oxidation in Chemical Mechanisms. *Arch. Biochem. Biophys.* **2011**, *507*, 126–134.

(57) Kumar, S. Engineering Cytochrome P450 Biocatalysts for Biotechnology, Medicine and Bioremediation. *Expert Opin. Drug Metab. & Toxicol.* **2010**, *6*, 115–131.

(58) Shaik, S.; Kumar, D.; de Visser, S. P.; Altun, A.; Thiel, W. Theoretical Perspective on the

View Article Online
DOI: 10.1039/D5CP02120K

Structure and Mechanism of Cytochrome P450 Enzymes. *Chem. Rev.* **2005**, *105*, 2279–2328.

(59) Pikuleva, I. A.; Waterman, M. R. Cytochromes P450: Roles in Diseases. *J. Biol. Chem.* **2013**, *288*, 17091–17098.

(60) Kadish, K. M.; Smith, K. M.; Guilard, R. *The Porphyrin Handbook*; Academic Press: San Diego, 2000.

(61) Liao, M. S.; Watts, J. D.; Huang, M. J. DFT Study of Unligated and Ligated Manganese(II) Porphyrins and Phthalocyanines. *Inorg. Chem.* **2005**, *44*, 1941–1949.

(62) Key, H. M.; Dydio, P.; Clark, D. S.; Hartwig, J. F. Abiological Catalysis by Artificial Haem Proteins Containing Noble Metals in place of Iron. *Nature* **2016**, *534*, 534–537.

(63) Furukawa, Y.; Ishimori, K.; Morishima, I. Electron Transfer Reactions in Zn-substituted Cytochrome P450cam. *Biochem.* **2000**, *39*, 10996–11004.

(64) Gelb, M. H.; Toscano, W. A.; Sligar, S. G. Chemical Mechanisms for Cytochrome P-450 Oxidation: Spectral and Catalytic Properties of a Manganese-substituted Protein. *Proc. Nat. Acad. Sci. USA* **1982**, *79*, 5758–5762.

(65) Kubota, R.; Takabe, T.; Arima, K.; Taniguchi, H.; Asayama, S.; Kawakami, H. New Class of Artificial Enzyme Composed of Mn-porphyrin, Imidazole, and Cucurbit[10]uril toward use as a Therapeutic Antioxidant. *J. Mat. Chem. B* **2018**, *6*, 7050–7059.

(66) Imran, M.; Ramzan, M.; Qureshi, A. K.; Azhar Khan, M.; Tariq, M. Emerging Applications of Porphyrins and Metalloporphyrins in Biomedicine and Diagnostic Magnetic Resonance Imaging. *Biosensors* **2018**, *8*, 1–17.

(67) Banerjee, A.; Shah, J. K. Insight into Conformationally-dependent Binding of 1-n-alkyl-3-methylimidazolium Cations to Porphyrin Molecules using Quantum Mechanical Calculations. *Phys. Chem. Chem. Phys.* **2019**, *21*, 10095–10104.

View Article Online
DOI: 10.1039/D5CP02120K

(68) Frisch, M. J.; Trucks, G. W.; Schlegel, H. B.; Scuseria, G. E.; Robb, M. A.; Cheeseman, J. R.; Scalmani, G.; Barone, V.; Mennucci, B.; Petersson, G. A. et al. Gaussian - 09 Revision E.01. Gaussian Inc. Wallingford CT 2009.

(69) Hehre, W. J.; Ditchfield, R.; Pople, J. A. Self—Consistent Molecular Orbital Methods. XII. Further Extensions of Gaussian—Type Basis Sets for Use in Molecular Orbital Studies of Organic Molecules. *J. Chem. Phys.* **1972**, *56*, 2257–2261.

(70) Banerjee, A.; Shah, J. K. Elucidating the Effect of the Ionic Liquid type and Alkyl Chain Length on the Stability of Ionic Liquid-Iron Porphyrin Complexes. *J. Chem. Phys.* **2020**, *153*.

(71) Hay, P. J.; Wadt, W. R. Ab initio Effective Core Potentials for Molecular Calculations. Potentials for the Transition Metal Atoms Sc to Hg. *J. Chem. Phys.* **1985**, *82*, 270–283.

(72) Shore, T. C.; Mith, D.; DePrekel, D.; McNall, S.; Ge, Y. A B3LYP Study on the C–H activation in Propane by Neutral and +1 Charged Low-energy Platinum Clusters with 2–6 atoms. *React. Kinet. Mech. Catal.* **2013**, *109*, 315–333.

(73) Blanco, R.; Orts, J. M. B3LYP Study of Water Adsorption on Cluster Models of Pt(111), Pt(100) and Pt(110): Effect of Applied Electric Field. *Electrochim. Acta* **2008**, *53*, 7796–7804.

(74) Glukhovtsev, M. N.; Bach, R. D.; Nagel, C. J. Performance of the B3LYP/ECP DFT Calculations of Iron-Containing Compounds. *J. Phys. Chem. A* **1997**, *101*, 316–323.

(75) Zhao, Y.; Truhlar, D. G. The M06 Suite of Density Functionals for Main Group Thermochemistry, Thermochemical Kinetics, Non-covalent Interactions, Excited States, and Transition Elements: Two New Functionals and Systematic Testing of Four M06-class Functionals and 12 other Functionals. *Theor. Chem. Acc.* **2008**, *120*, 215–241.

View Article Online
DOI: 10.1039/D5CP02120K

(76) Cramer, C. J.; Truhlar, D. G. Density Functional Theory for Transition Metals and Transition Metal Chemistry. *Phys. Chem. Chem. Phys.* **2009**, *11*, 10757–10816.

(77) Lu, X.; Ahsaine, H. A.; Dereli, B.; Garcia-Esparza, A. T.; Reinhard, M.; Shinagawa, T.; Li, D.; Adil, K.; Tchalala, M. R.; Kroll, T. et al. Operando Elucidation on the Working State of Immobilized Fluorinated Iron Porphyrin for Selective Aqueous Electroreduction of CO2to CO. *ACS Catalysis* **2021**, *11*, 6499–6509.

(78) Ali, M. E.; Sanyal, B.; Oppeneer, P. M. Electronic structure, spin-states, and spin-crossover reaction of heme-related fe-porphyrins: A theoretical perspective. *Journal of Physical Chemistry B* **2012**, *116*, 5849–5859.

(79) Tian, B.; Eriksson, E. S.; Eriksson, L. A. Can range-separated and hybrid DFT functionals predict low-lying excitations? A Tookad case study. *Journal of Chemical Theory and Computation* **2010**, *6*, 2086–2094.

(80) Kepenekian, M.; Calborean, A.; Vetere, V.; Guennic, B. L.; Robert, V.; Maldivi, P. Toward reliable DFT investigations of Mn-porphyrins through CASPT2/DFT comparison. *Journal of Chemical Theory and Computation* **2011**, *7*, 3532–3539.

(81) Radoń, M. Role of Spin States in Nitric Oxide Binding to Cobalt(II) and Manganese(II) Porphyrins. is Tighter Binding Always Stronger? *Inorganic Chemistry* **2015**, *54*, 5634–5645.

(82) Parr, R. G.; Szentpály, L. v.; Liu, S. Electrophilicity Index. *J. Am. Chem. Soc.* **1999**, *121*, 1922–1924.

(83) O'boyle, N. M.; Tenderholt, A. L.; Langner, K. M. cclib: A Library for Package-independent Computational Chemistry Algorithms. *J. Comput. Chem.* **2008**, *29*, 839–845.

(84) Bultinck, P.; Carbó-Dorca, R.; Langenaeker, W. Negative Fukui functions: New Insights Based on Electronegativity Equalization. *J. Chem. Phys.* **2003**, *118*, 4349–4356.

View Article Online
DOI: 10.1039/D5CP02120K

(85) Fuentealba, P.; Pérez, P.; Contreras, R. On the Condensed Fukui Function. *Journal of Chemical Physics* **2000**, *113*, 2544–2551.

(86) Hirshfeld, F. L. Bonded-Atom Fragments for Describing Molecular Charge Densities. *Theoret. Claim. Acta (Berl.)* **1977**, *44*, 129–138.

(87) Bultinck, P.; Alsenoy, C. V.; Ayers, P. W.; Carbó-Dorca, R. Critical Analysis and Extension of the Hirshfeld Atoms in Molecules. *J. Chem. Phys.* **2007**, *126*.

(88) Reed, A. E.; Weinstock, R. B.; Weinhold, F. Natural Population Analysis. *J. Chem. Phys.* **1985**, *83*, 735–746.

(89) Reed, A. E.; Curtiss, L. A.; Weinhold, F. Intermolecular Interactions from a Natural Bond Orbital, Donor-Acceptor Viewpoint. *Chem. Rev.* **1988**, *88*, 899–926.

(90) Glendening, E. D.; Landis, C. R.; Weinhold, F. Natural bond orbital methods. *Wiley Interdiscip. Rev. Comput. Mol. Sci.* **2012**, *2*, 1–42.

(91) Zhou, Z.; Shen, M.; Cao, C.; Liu, Q.; Yan, Z. Opposing influences of ruffling and doming deformation on the 4-N cavity size of porphyrin macrocycles: The role of heme deformations revealed. *Chemistry - A European Journal* **2012**, *18*, 7675–7679.

(92) Simonneaux, G.; Bondon, A. Mechanism of Electron Transfer in Heme Proteins and Models: The NMR Approach. *Chem. Rev.* **2005**, *105*, 2627–2646.

(93) Maes, E. M.; Roberts, S. A.; Weichsel, A.; Montfort, W. R. Ultrahigh Resolution Structures of Nitrophorin 4: Heme Distortion in Ferrous CO and NO Complexes. *Biochem.* **2005**, *44*, 12690–12699.

(94) Zhou, Z.; Liu, Q.; Yan, Z.; Long, G.; Zhang, X.; Cao, C.; Jiang, R. Conversion of Electron Configuration of Iron Ion through Core Contraction of Porphyrin: Implications for Heme Distortion. *Org. Lett.* **2013**, *15*, 606–609.

View Article Online
DOI: 10.1039/D5CP02120K

(95) Jentzen, W.; Unger, E.; Karvounis, G.; Shelnutt, J. A.; Dreybrodt, W.; Schweitzer-Stenner, R. Conformational Properties of Nickel(II) Octaethylporphyrin in Solution. 1. Resonance Excitation Profiles and Temperature Dependence of Structure-sensitive Raman Lines. *J. Phys Chem.* **1996**, *100*, 14184–14191.

(96) Huang, Q.; Medforth, C. J.; Schweitzer-Stenner, R. Nonplanar heme deformations and excited state displacements in nickel porphyrins detected by Raman spectroscopy at soret excitation. *Journal of Physical Chemistry A* **2005**, *109*, 10493–10502.

(97) Jentzen, W.; Song, X. Z.; Shelnutt, J. A. Structural Characterization of Synthetic and Protein-bound Porphyrins in Terms of the Lowest-frequency Normal Coordinates of the Macrocycle. *J. Phys. Chem. B* **1997**, *101*, 1684–1699.

(98) Jentzen, W.; Ma, J. G.; Shelnutt, J. A. Conservation of the Conformation of the Porphyrin Macrocycle in Hemoproteins. *Biophys. J.* **1998**, *74*, 753–763.

(99) Kingsbury, C. J.; Senge, M. O. The Shape of Porphyrins. *Coord. Chem. Rev.* **2021**, *431*.

(100) Feng, X.; Yu, J.; Lei, M.; Fang, W.; Liu, S. Toward Understanding Metal-Binding Specificity of Porphyrin : A Conceptual Density Functional Theory Study. *J. Phys. Chem. B.* **2009**, 13381–13389.

(101) Durrant, M. C. A computational study of ligand binding affinities in iron(iii) porphine and protoporphyrin IX complexes. *Dalton Transactions* **2014**, *43*, 9754–9765.

(102) Olsson, S.; Dahlstrand, C.; Gogoll, A. Design of oxophilic metalloporphyrins: An experimental and DFT study of methanol binding. *Dalton Transactions* **2018**, *47*, 11572–11585.

(103) Salmahaminati; Abe, M.; Purnama, I.; Mulyana, J. Y.; Hada, M. Density Functional Study of Metal-to-Ligand Charge Transfer and Hole-Hopping in Ruthenium(II) Complexes with Alkyl-Substituted Bipyridine Ligands. *ACS Omega* **2021**, *6*, 55–64.

View Article Online
DOI: 10.1039/D5CP02120K

(104) Kozlowski, P. M.; Bingham, J. R.; Jarzecki, A. A. Theoretical Analysis of Core Size Effect in Metalloporphyrins †. **2008**, 12781–12788.

(105) Liao, M.-S.; Scheiner, S. Electronic structure and bonding in metal porphyrins, metal= Fe, Co, Ni, Cu, Zn. *The Journal of chemical physics* **2002**, *117*, 205–219.

(106) Liao, M.-S.; Scheiner, S. Comparative study of metal-porphyrins,-porphyrazines, and-phthalocyanines. *Journal of Computational Chemistry* **2002**, *23*, 1391–1403.

(107) Sessler, J. L.; Tomat, E. Transition-metal complexes of expanded porphyrins. *Accounts of chemical research* **2007**, *40*, 371–379.

(108) Wei, Y.; Liang, Y.; Wu, Q.; Xue, Z.; Feng, L.; Zhang, J.; Zhao, L. Effects of tuning the structural symmetry of cobalt porphyrin on electrocatalytic oxygen reduction reactions. *Dalton Transactions* **2023**, *52*, 14573–14582.

(109) Bansal, D.; Ghahramanzadehasl, H.; Cardenas-Morcoso, D.; Desport, J.; Frache, G.; Bengasi, G.; Boscher, N. D. Directly-Fused Ni (II) Porphyrin Conjugated Polymers with Blocked meso-Positions: Impact on Electrocatalytic Properties. *Chemistry–A European Journal* **2024**, *30*, e202400665.

View Article Online
DOI: 10.1039/D5CP02120K

The data supporting this article have been included as part of the Supplementary Information. Sample of an input file, output file, and analysis script will be made available via GitHub.